Received: 11 January 2023 | Revised: 3 June 2023 | Accepted: 15 August 2023

DOI: 10.1049/cth2.12544

IET Control Theory & Applications

The Institution of Engineering and Technology WILEY

ORIGINAL RESEARCH

Active fault-tolerant load frequency control for multi-area power systems with electric vehicles under deception attacks

Xinghua Liu[1] | Yuru Liang[1] | Siwei Qiao[1] | Guoqing Yang[1] | Peng Wang[2]

[1]School of Electrical Engineering, Xi'an University of Technology, Xi'an, China

[2]School of Electrical and Electronic Engineering, Nanyang Technological University, Singapore, Singapore

Correspondence
Xinghua Liu, School of Electrical Engineering, Xi'an University of Technology, Xi'an 710048, China.
Email: liuxh@xaut.edu.cn

Funding information
National Natural Science Foundation of China, Grant/Award Number: U2003110

Abstract

This paper studies the active fault tolerant load frequency control of multi-area power systems with electric vehicles under deception attacks. An integrated design of fault estimation and fault-tolerant control is proposed to guarantee the stability of the system under sensor faults and deception attacks. Considering the uncertainty caused by the demand of the owner and the state of the battery, a multi-area power system model is proposed. Then, an active fault tolerant load frequency control scheme is designed. The proportional-derivative sliding mode observer is used to estimate the fault and system status in real-time. During the fault occurrence, the estimated value obtained by the observer is utilized to design the controller without any fault diagnosis scheme, which simplifies the controller design process. A sufficient Lyapunov-Krasovskii criterion is derived to ensure the stability performance of the multi-area power system. Finally, simulation examples are provided for a three-area power system contains electric vehicles, and the results prove the correctness and feasibility of the proposed fault-tolerant control scheme.

1 | INTRODUCTION

Frequency deviates from nominal values directly affect the operation, safety and reliability of the system [1]. Load frequency control (LFC) is an important part of automatic power generation control (AGC). It has been proven to be very effective in controlling power system frequency stabilization [2–6]. In recent years, a large number of electric vehicles have been injected into the grid due to environmental pollution and the depletion of fossil fuels. However, the random and uncoordinated charging of electric vehicles will increase the demand in the power system [7]. With the development of vehicle-to-grid (V2G) technology, the EVs are used to participate in the frequency regulation of power systems because the battery of EVs have the characteristics of faster response and adjustment speed than traditional generator sets [8]. In [9], the authors studied the participation of EVs in smart grid frequency regulation as controllable loads. The results show that EVs have the sufficient frequency regulation capability. Due to the limited capacity of a single EVs, a large number of EV participating system frequency modulation should be aggregated by an EV Aggregator (EVA) [10]. In [11], the authors proposed an integrated EVs management method developed by EV aggregators, which can manage the charge/discharge operations of EVs fleets and provide frequency re-services. The battery's state of charge (SOC) is the ratio between stored energy and its capacity, which is an important feature of EVs [12]. In fact, when EVs take part in frequency regulation of the power system, we should also consider the requirements of the owners. Therefore, the SOC value of EVs should be controlled within a reasonable range. SOC is closely related to EVs gain, which determines EVs output power deviation [13]. Besides, EVs gain should vary within the expected range. In related studies, EVs gain is simply treated as constant [14–16]. A robust frequency control scheme was proposed in [17] for the power system model in which the uncertainty caused by the change of battery state of charge was considered. However, modern power networks are often in harsh environments such as high voltage and high magnetic field, leading to the failure of related actuators, sensors and controller modules. This may cause the system to lose the expected performance index and cause huge losses, but such problems are not considered in the above literature.

Fault tolerant control can ensure the safe operation of the controlled system when faults occur [18]. Among related

researches, fault-tolerant control was used in different areas, such as islanded microgrids [19], satellite attitude control systems [20], wind turbines [21], and battery storage systems [22]. Therefore, we propose fault tolerant load frequency control to improve the safety and reliability of power system. In [23], the fault tolerant load frequency control scheme with known and unknown actuator faults was designed for multi-area wind power generation system. In [24], the authors constructed a novel actuator fault model in which contains linear and nonlinear terms, and a corresponding fault-tolerant control scheme was proposed to analyze the performance of the novel model. However, the [23] and [24] adopts passive fault-tolerant control (PFTC), which is highly limited and only effective for known faults. On the contrary, after detecting the fault information of the controlled system in the fault detection and identification link, the active fault-tolerant control (AFTC) adjusts the structure and parameters of the controlled system online to achieve the desired performance index. It can achieve better robustness and fault acceptability than PFTC [20]. In [25], the AFTC problems of the multi-area power system under sensor fault was studied. In [26], AFTC based on interval observer was designed to solve the problem of LFC and sensor fault tolerance control in power grid. However, these methods require a fault diagnosis scheme that is sensitive to changes in model parameters and operating conditions. This paper mainly introduces the integrated design of fault estimation (FE) and AFTC, which can directly estimate the fault component of the system. When the fault estimate value is non-zero, the fault diagnosis result is automatically indicated and there is no need for additional complex fault diagnosis scheme.

Modern power systems usually use open communication networks. Therefore, it is more vulnerable to communication channel interference, false data injection, load change of power system and other malicious attacks [27]. Deception attacks destroy data integrity by replacing the normally transmitted data in the communication channel with fake data [28]. It poses a great threat to the safe operation of power system. At present, there has been increasing attention to the study of deception attacks [29–31]. The load frequency control problem of networked power system with random deception attack and limited bandwidth was studied [29]. In [30], the problem of load frequency control under mixed network attacks was studied. The security control of large-scale systems under joint attacks was studied in [31]. The considered attacks could happen in both sensor-to-observer and controller-to-actuator. It is worth noting that the LFC problem of multi-area power systems with electric vehicles that involve sensor faults and deception attacks has not been well studied, which is the motivation for this paper.

In this paper, an active fault-tolerant LFC strategy is proposed for multi-area power systems with EVs under deception attacks and sensor faults. The main contributions of this paper can be outlined as follows:

1) A power system model including electric vehicles, deception attack and sensor fault is built. Compared with [14–16], the EVs model considers the demands of EV owners and the impact of SOC.
2) A proportional-derivative sliding mode observer is applied to integrate the design of fault estimation and fault tolerance control. Compared with [26], the observer is used to estimate the fault and system state simultaneously, which does not require additional complicated fault diagnosis.
3) A multiple Lyapunov function is constructed, and then the stability criterion of the multi-area power system is established by Lyapunov theory and matrix inequalities, where the obtained result is less conservative than that of [25].

The rest of this paper is organized as follows. In Section 2, we present our problem statement and some technical preliminaries. Our main theoretic framework and proofs are presented in Section 3. Numerical examples and simulations are presented to verify our methods in Section 4. Finally, Section 5 concludes the paper.

2 | PROBLEM FORMULATION

In recent years, due to the gradual depletion of fossil fuels, EVs have been widely used. Aggregated electric vehicles can be used to participate in frequency regulation of the power system. When the grid load is too high, the EVs are discharged to the grid. When the grid load is too low, the EVs are charged by the grid to ensure the stability of the system frequency. Because the power provided by one EV is too low, the EVA is used to aggregate and control a large number of EVs. Firstly, the EVA collects information about the EVs from the charging-discharging stations and sends it to the LFC control center. Then the control center processes the information to make a decision and sends the command to the EVA. Finally, the EVA controls the orderly charging and discharging of the EVs according to the adjustment command. Thereby achieving the purpose of frequency regulation, as shown in Figure 1.

2.1 | Electric vehicle model

The information contains the minimum expected battery charge to leave the grid SOC_{exp}, the dwell time T_p, and the initial SOC of the battery SOC_0. The charging time of an electric vehicle from SOC_0 to SOC_{exp} can be expressed as

$$T_{ct} = \frac{Q_{ev}(SOC_{exp} - SOC_0)}{\eta_c P_{lim}}, \tag{1}$$

where Q_{ev} is the battery capacity of EVs, η_c is the charging efficiency, P_{lim} is the limitation of EVs charging and discharging power. Obviously, only if $T_{ct} < T_p$, the EVs can provide frequency regulation service.

The deviation of power output for the i_{th} EV battery system is described by

$$\dot{P}_{ei}(t) = -\frac{1}{T_{ei}} P_{ei}(t) + \frac{K_{ei}}{T_{ei}} u_i(t), \tag{2}$$

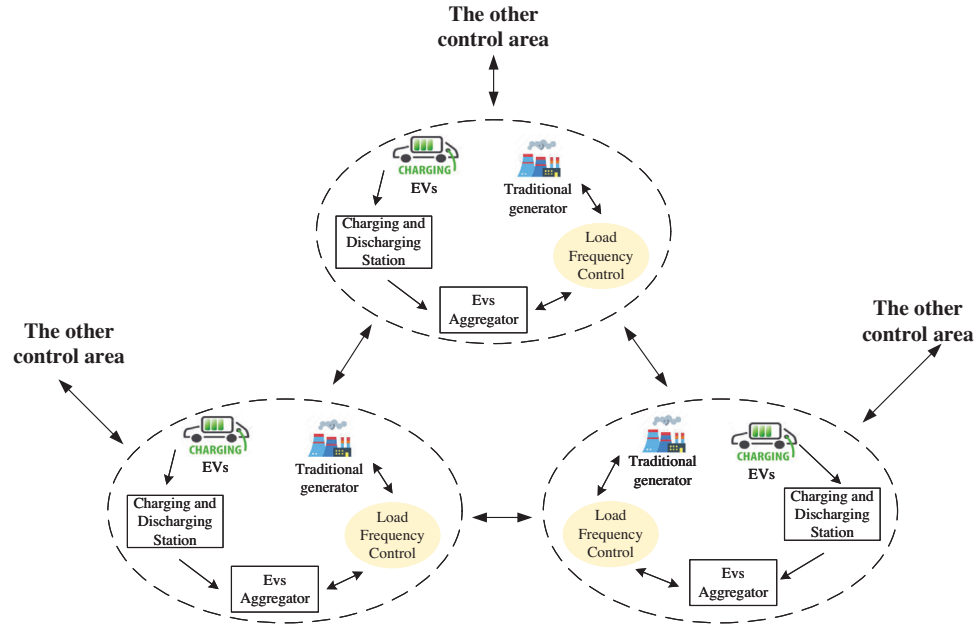

FIGURE 1 Multi-area power systems with electric vehicles.

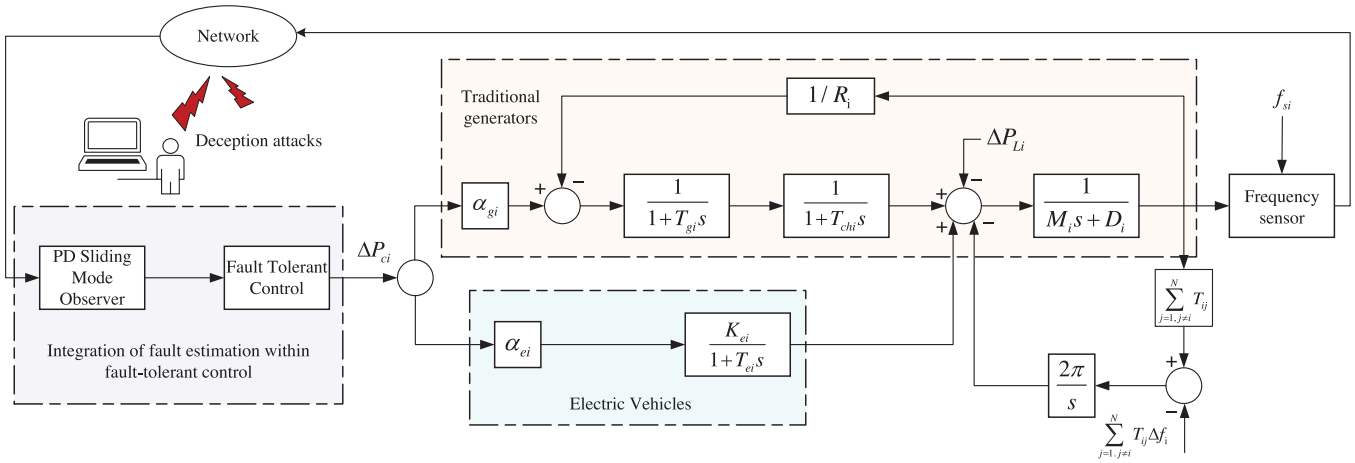

FIGURE 2 Dynamic model of the *i*th in multi-area power scheme.

where we assume that all EVs have the same time-constant T_{ei}, K_{ei} is the EV gain and the system input $u(t)$ is reallocated equally to each EV as $u_i(t) = u(t)/N$. And N is the total number of EVs. Accordingly, the aggregated EVs can be modeled as a first-order dynamic model. Hence, the deviation of power output for the aggregated EVs is obtained as

$$\dot{P}_e(t) = -\frac{1}{T_e}P_e(t) + \frac{K_e}{T_e}u(t), \tag{3}$$

where aggregated EVs gain is $K_e = \frac{\sum_{i=1}^{N} K_{ei}}{N}$.

Individual EV gain K_{ei} is determined by frequency and battery SOC. To prevent overcharging (over discharging), if the SOC is almost full (almost empty), no high power charging (discharging) should be done. Therefore EV gain K_{ei} is modeled as

$$\left\{ K_{ei} = K_m\left(1 - \left(\frac{SOC_i - SOC_{low(high),i}}{SOC_{max(min),i} - SOC_{low(high),i}}\right)^2\right), \tag{4}$$

where K_m is the maximum gain of EV, and SOC_i, $SOC_{low,i}$, $SOC_{high,i}$, $SOC_{min,i}$ and $SOC_{max,i}$ denote the current, known low and high, known minimum and maximum battery SOC of the i_{th} EV, respectively. Therefore, K_{ei} is

$$K_{ei} = K_m - K_m g_i(t). \tag{5}$$

Assuming that at any time t, there are N EVs participating in the multi-area power system, the aggregated EVs gain can be

obtained as

$$K_e = \frac{\sum_{i=1}^{N} K_{ei}}{N} = K_m - g(t)K_m, \tag{6}$$

where $g_i(t)$ is a time-varying function related to the current SOC value.

$$g_i(t) = \left(\frac{SOC_i - SOC_{low(high),i}}{SOC_{max(min),i} - SOC_{low(high),i}} \right)^2, \tag{7}$$

and $g(t) = \sum_{i=1}^{N} g_i(t)/N$ is the average of N different values $g_i(t)$.

Therefore, the power output deviation of the aggregated EVs can be obtained

$$\dot{P}_e(t) = -\frac{1}{T_e}P_e(t) + \frac{K_m}{T_e}u(t) - \frac{g(t)K_m}{T_e}u(t). \tag{8}$$

2.2 | Power system model with sensor fault

The i_{th} area multi-area electric power system simplified model is given in Figure 2. Based on signal transmission, the dynamic equation of the system can be obtained as follows

$$\begin{cases} \Delta\dot{f}_i(t) = \frac{1}{M_i}(\Delta P_{mi}(t) + \Delta P_{ei}(t) - \Delta P_{tie-i}(t) \\ \qquad - \Delta P_{L,i}(t)) - \frac{D_i}{M_i}\Delta f_i(t) \\ \Delta\dot{P}_{mi}(t) = \frac{1}{T_{mi}}(\Delta P_{gi}(t) - \Delta P_{mi}(t)) \\ \Delta\dot{P}_{gi}(t) = \frac{1}{T_{gi}}(u(t) - \Delta P_{gi}(t) - \frac{1}{R_i}\Delta f_i(t) \\ \qquad - \Delta ACE_i(t - h(t))) \\ \Delta\dot{P}_{ei}(t) = -\frac{1}{T_{ei}}P_{ei}(t) + \frac{K_{mi}}{T_{ei}}u(t) - \frac{g(t)K_{mi}}{T_{ei}}u(t) \\ \int ACE_i(t) = k_i\beta_i\Delta f_i + k_i\Delta P_{tie-i} \\ \Delta\dot{P}_{tie-i}(t) = 2\pi \sum_{j=1,i\neq 1}^{N} \Delta T_{ij}\Delta f_i \end{cases}, \tag{9}$$

where the meaning of the symbols are listed in Table 1.

Remark 1. The multi-area power system consists of the conventional generator and the EVA. The traditional generator consists of generator, turbine and governor. According to Figure 2, the transfer function of the power system can be obtained. By applying the Laplace transform of the transfer function, Equation (9) can be obtained. The treatment method can be referred to [3, 4].

TABLE 1 Symbols of the system model.

Δf_i	Frequency deviation
ΔP_{mi}	Mechanical power change
ΔP_{ei}	EVs output power change
ΔP_{gi}	Governor output change
$\Delta P_{L,i}$	Disturbance of load
M_i	Equivalent inertia constant
D_i	Equivalent damping coefficient
T_{gi}	Time-constant of governor
T_{mi}	Time-constant of turbine
T_{ei}	Time-constant of EVs
R_i	Speed droop
β_i	Frequency bias factor
ΔP_{tie-i}	Power deviation of tie-line
K_{mi}	The maximum gain of EVs
T_{ij}	Synchronizing coefficient of tie-line

Thus, the state space function can be represented as

$$\begin{cases} \dot{x}(t) = Ax(t) + A_d x(t - h(t)) + (B + \Delta B(t))u(t) \\ \qquad + Dw(t) \\ y(t) = Cx(t), \end{cases} \tag{10}$$

where

$$x_i(t) = \left[\triangle f_i \;\; \triangle P_{mi} \;\; \triangle P_{gi} \;\; \triangle P_{ei} \;\; \triangle P_{tie-i} \;\; \int ACE_i \right]^T,$$

$$y_i(t) = \left[ACE_i \;\; \int ACE_i \right]^T, \omega_i(t) = \Delta P_{L,i},$$

$$A = \begin{bmatrix} -\frac{D}{M} & 0 & \frac{1}{M} & \frac{1}{M} & 0 & 0 \\ -\frac{1}{R_g T_g} & -\frac{1}{T_g} & 0 & 0 & 0 & 0 \\ 0 & \frac{1}{T_g} & -\frac{1}{T_g} & 0 & 0 & 0 \\ 0 & 0 & 0 & -\frac{1}{T_e} & 0 & 0 \\ 2\pi \sum_{j=1,i\neq 1}^{N} \Delta T_{ij} & 0 & 0 & 0 & 0 & 0 \\ \beta & 0 & 0 & 0 & 1 & 0 \end{bmatrix},$$

$$A_d = \begin{bmatrix} 0_{2x5} & 0_{2x1} \\ 0_{1x5} & -\frac{1}{T_{gi}} \\ 0_{3x5} & 0_{3x1} \end{bmatrix}, B = \begin{bmatrix} 0 & \frac{\alpha_{gi}}{T_{gi}} & 0 & \frac{\alpha_{ei}K_{mi}}{T_{ei}} & 0 & 0 \end{bmatrix}^T,$$

$$\Delta B(t) = Hg(t)E, H = \begin{bmatrix} 0 & 0 & 0 & -\frac{K_{mi}}{T_e} & 0 & 0 \end{bmatrix}^T,$$

$$E = [1\ 0\ 0\ 0\ 0\ 0], D = [-1/M\ 0\ 0\ 0\ 0\ 0]^T,$$

$$\bar{C} = \begin{bmatrix} \beta & 0 & 0 & 0 & 1 & 0 \\ 0 & 0 & 0 & 0 & 0 & 1 \end{bmatrix}.$$

Considering the existence of delay in actual transmission, $h(t)$ is defined to represent the time delay. And $h(t)$ is a time-varying differentiable function as follows

$$0 \le h(t) \le \bar{h},\ 0 \le \dot{h}(t) \le \phi \le 1.$$

Considering the influence of sensor failure, the system state equation can be rewritten as

$$\begin{cases} \dot{x}(t) = Ax(t) + A_d x(t - h(t)) + (B + \Delta B(t))u(t) \\ \qquad + Dw(t) \\ y(t) = Cx(t) + f_s(t) \end{cases}, \quad (11)$$

where $f_s(t)$ represents the sensor fault, which is satisfies $\|f_s(t)\| \le \alpha$ and α is a known constant [25].

2.3 | Deception attack

Compared to traditional, modern deregulated power system load frequency control schemes use open communication facilities. The output signal under deception attacks can be described as

$$y(t) = Cx(t) + f_s(t) + f_{ag}(t), \quad (12)$$

where $f_{ag}(t)$ stands for the deception attack launched by the adversary.

From the attacker's point of view, they are more willing to attack when the system is stable than when the system state close to stable situation. Therefore the system remains unstable for a long time, the attack status is as follows

$$f_{ag}(t) = \begin{cases} -aCx(t) + \varphi(t) & |\Delta f_i| < \upsilon \\ 0 & otherwise \end{cases}, \quad (13)$$

where $\varphi(t)$ is an unknown-but-bounded injected signal satisfying $\|\varphi(t)\| \le \sigma$. a, σ and υ are given positive scalars. When the system frequency satisfies $|\Delta f_i| < \upsilon$, the system is considered stable and the adversary sends an attack signal.

Therefore, the system state space function can be expressed as

$$\begin{cases} \dot{x}(t) = Ax(t) + A_d x(t - h(t)) + (B + \Delta B(t))u(t) \\ \qquad + D\omega(t) \\ y(t) = Cx(t) + f_s(t) + f_{ag}(t) \end{cases}. \quad (14)$$

Before proceeding with the main results, we present the following definition and lemmas, which play an important role in the proof of the main result.

Definition 1. For $w(t) = 0$, if there is a continuous first-order partial derivative of $V(t)$, and $V(t)$ is positively definite and $\dot{V}(t)$ is negatively definite, then the system (14) is asymptotically stable. Besides, H_∞ performance is guaranteed under the condition of zero initial state, if the inequality $\|y(t)\|_2 \le \gamma\|w(t)\|_2$ holds, in which $\gamma > 0$ is a pregiven constant.

Lemma 1 [32]. *For a positive definite matrix $R > 0$, any continuously differentiable function $x : [a, b] \longrightarrow \mathbb{R}^n$, the following inequality holds*

$$\int_a^b \dot{x}^T(s) R \dot{x}(s) \ge \frac{1}{b-a} \delta \tilde{R} \delta,$$

where $\tilde{R} = \mathrm{diag}\{R, 3R, 5R\}$ and

$$\delta = \mathrm{col}\left\{ x(b) - x(a), x(b) + x(a) - \frac{2}{b-a}\int_a^b x(s)\mathrm{d}s, x(b) \right.$$
$$\left. -x(a) - \frac{6}{b-a}\int_a^b x(s)\mathrm{d}s \right\}.$$

Lemma 2 [33]. *For any $x, y \in \mathbb{R}$ and positive scalar ε, we have*

$$2y^T x \le \varepsilon x^T x + \frac{1}{\varepsilon} y^T y.$$

3 | MAIN RESULTS

3.1 | PD sliding mode observer design

An efficient observer is proposed for the extended system (14), which can estimate both the original state and the sensor fault value.

In order to facilitate further analysis, the following matrix is constructed

$$E = \begin{bmatrix} I_n & 0 & 0 \\ 0 & I_p & 0 \\ 0 & 0 & 0 \end{bmatrix}, \bar{A} = \begin{bmatrix} A & 0 & 0 \\ 0 & -I_p & 0 \\ 0 & 0 & -I_q \end{bmatrix},$$

$$\bar{B} = \begin{bmatrix} B \\ 0 \\ 0 \end{bmatrix}, \Delta\bar{B} = \begin{bmatrix} \Delta B \\ 0 \\ 0 \end{bmatrix}, \bar{D} = \begin{bmatrix} D \\ 0 \\ 0 \end{bmatrix},$$

$$\bar{C}=\begin{bmatrix} C \\ I_p \\ I_q \end{bmatrix}^T, N=\begin{bmatrix} 0 & 0 \\ I_p & 0 \\ 0 & I_q \end{bmatrix}, G_1=\begin{bmatrix} 1 \\ 0 \end{bmatrix}^T,$$

$$G_2=\begin{bmatrix} 0 \\ 1 \end{bmatrix}^T, \bar{f}=\begin{bmatrix} f_s+\dot{f}_s \end{bmatrix}, \bar{x}(t)=\begin{bmatrix} x(t) \\ f_s(t) \\ f_{ag}(y(t)) \end{bmatrix}.$$

Then, an augmented state space function based on (14) can be obtained

$$\begin{cases} E\dot{\bar{x}}(t)=\bar{A}\bar{x}(t)+A_d x(t-h(t))+(\bar{B}+\Delta\bar{B}(t))u(t) \\ \qquad +NG_1\bar{f}(t)+NG_2 f_{ag}(t)+\bar{D}w(t) \\ y(t)=\bar{C}\bar{x}(t) \end{cases}. \quad (15)$$

It can be observed that the matrices satisfies the following properties

$$\text{rank}\begin{bmatrix} E \\ \bar{C} \end{bmatrix}=\text{rank}\begin{bmatrix} I_n & 0 \\ 0 & 0 \\ C & I_p \end{bmatrix}=n+p.$$

There exists a matrix $\bar{L}_D=[0_{p\times n} \ W]^T$ such that the matrix $\bar{S}$ is nonsingular

$$\bar{S}=(E+\bar{L}_D\bar{C}).$$

Now, the PD sliding mode observer-based power system model can be given as

$$\begin{cases} \bar{S}\dot{\bar{z}}(t)=(\bar{A}-\bar{L}_P\bar{C})\hat{\bar{x}}(t)+(\bar{A}_d-\bar{L}_H\bar{C})\hat{\bar{x}}(t-h(t)) \\ \qquad +(\bar{B}+\Delta\bar{B}(t))u(t)+\bar{L}_P y(t) \\ \qquad +\bar{L}_H y(t-h(t))+\bar{L}_s u_s(t)+\bar{D}w(t) \\ \hat{\bar{x}}(t)=\bar{z}(t)+\bar{S}^{-1}\bar{L}_D y(t) \end{cases}, \quad (16)$$

where $\bar{z}(t)=[z_x^T(t), z_s^T(t)]^T$ denotes the intermediate variable and $\hat{\bar{x}}(t)=[\hat{x}^T(t), \hat{f}_s^T(t)]^T$ denotes the estimation of $\bar{x}(t)$, $\bar{L}_P$, $\bar{L}_D$, $\bar{L}_s$ represent the observer gains. What is more, $u_s(t)$and $\bar{L}_s$ are designed to eliminate the effects of sensor failure and keep the system stable.

Remark 2. The fault diagnosis is sensitive to the change of model parameters and operating conditions, but the system state and fault signal can be estimated simultaneously by PD sliding mode observer. When the fault estimate is non-zero, it indicates that the system has failed. Therefore, there is no need to design additional complex fault diagnosis scheme. In addition, PD sliding mode observer has the advantages of fast response, good transient performance and insensitivity to interference. Based on the above description, PD sliding mode observer is widely used to solve fault tolerance problems [25, 34].

Based on (16), we have

$$\begin{aligned} \bar{S}\ddot{\hat{\bar{x}}}(t)=&(\bar{A}-\bar{L}_P\bar{C})\dot{\hat{\bar{x}}}(t)+(\bar{A}_d-\bar{L}_H\bar{C})\dot{\hat{\bar{x}}}(t-h(t)) \\ &+(\bar{B}+\Delta\bar{B}(t))\dot{u}(t)+\bar{L}_P\dot{y}(t)+\bar{L}_s\dot{u}_s(t) \\ &+\bar{L}_H\dot{y}(t-h(t))+\bar{L}_D\ddot{y}(t)+\bar{D}\dot{w}(t). \end{aligned} \quad (17)$$

Similarly, adding $\bar{L}_D\ddot{y}(t)$ on both sides of (15), we can get

$$\begin{aligned} \bar{S}\dot{\bar{x}}(t)=&(\bar{A}-\bar{L}_P\bar{C})\bar{x}(t)+(\bar{A}_d-\bar{L}_H\bar{C})\hat{\bar{x}}(t-h(t)) \\ &+(\bar{B}+\Delta\bar{B}(t))u(t)+\bar{L}_P y(t)+NG_1\bar{f}(t) \\ &+\bar{L}_H y(t-h(t))+NG_2 f_{ag}(t) \\ &+\bar{L}_D\ddot{y}(t)+\bar{D}\dot{w}(t). \end{aligned} \quad (18)$$

Furthermore, defining $\bar{e}(t)=\hat{\bar{x}}(t)-\bar{x}(t)$ and subtracting (17) to (18), we can obtain that

$$\begin{aligned} \bar{S}\dot{\bar{e}}(t)=&\bar{S}\ddot{\hat{\bar{x}}}(t)-\bar{S}\dot{\bar{x}}(t) \\ =&(\bar{A}-\bar{L}_P\bar{C})\bar{e}(t)+(\bar{A}-\bar{L}_H\bar{C})\bar{e}(t-h(t)) \\ &-NG_1\bar{f}(t)-NG_2 f_{ag}(t)+\bar{L}_s\dot{u}_s(t). \end{aligned} \quad (19)$$

The sliding mode surface is first defined as follows

$$s_e=\bar{N}^T\bar{S}^{-T}P\bar{e}(t), \quad (20)$$

and for each positive P is designed to satisfy $\bar{N}^T\bar{S}^{-T}P=H\bar{C}$. For further, $u_s(t)$ is designed as

$$u_s(t)=(-\lambda+G_1\alpha+G_2\sigma)sgn(s_e(t)). \quad (21)$$

3.2 | Active fault-tolerant controller design

A proportional differential sliding mode observer is designed which can simultaneously estimate system status and fault value. Next, the main work is to design a fault-tolerant controller to stabilize the system frequency.

Using $A\hat{C}E$ as the input of the controller, the PI-type controller is designed as follows

$$\begin{aligned} u(t) =& K_p A\hat{C}E(t) + K_I \int A\hat{C}E(t) \\ =& K\hat{y}(t) = KC\hat{x}(t). \end{aligned} \tag{22}$$

Therefore, the system state function (14) can be rewritten as

$$\begin{aligned} \dot{x}(t) =& Ax(t) + A_d x(t-\tau(t)) + (B+\Delta B(t))u(t) + Dw(t) \\ =& Ax(t) + A_d x(t-\tau(t)) + (B+\Delta B(t))(KC\hat{x}(t)) \\ &+ Dw(t) \\ =& Ax(t) + A_d x(t-\tau(t)) + (B+\Delta B(t))KCx(t) \\ &- (B+\Delta B(t))KCx(t) + (B+\Delta B(t))KC\hat{x}(t) \\ &+ Dw(t) \\ =& (A + (B+\Delta B(t))KC)x(t) + A_d x(t-\tau(t)) \\ &+ (B+\Delta B(t))KCe_x(t) + Dw(t) \\ =& (A + (B+\Delta B(t))KC)x(t) + A_d x(t-\tau(t)) \\ &+ (B+\Delta B(t))KCUe(t) + Dw(t). \end{aligned} \tag{23}$$

Then, the overall closed-loop multi-area power system is formulated in the following form

$$\begin{cases} \dot{x}(t) = (A + (B+\Delta B(t))KC)x(t) + A_d x(t-\tau(t)) \\ \qquad\quad + (B+\Delta B(t))KCU\bar{e}(t) + Dw(t) \\ \bar{S}\dot{\bar{e}}(t) = (\bar{A} - \bar{L}_P\bar{C})\bar{e}(t) + (\bar{A} - \bar{L}_H\bar{C})\bar{e}(t-\tau(t)) \\ \qquad\quad - NG_1\bar{f}(t) - NG_2 f_{ag}(t) + \bar{L}_s u_s(t) \end{cases}. \tag{24}$$

3.3 | Stability analysis

To facilitate in presenting our conditions, we denote

$$\eta(t) = \left[x(t) \quad \int_{t-h}^{t} x(s)\mathrm{d}s \quad \int_{t-h}^{t}\int_{s}^{t} x(u)\mathrm{d}u\mathrm{d}s\right]^T,$$

$$\varsigma(t) = [x(t) \quad \dot{x}(t) \quad x(t-h(t)) \quad x(t-h) \quad \frac{1}{h}\int_{t-h}^{t} x(s)\mathrm{d}s \quad \bar{e}(t) \quad \bar{e}(t-h) \quad \bar{e}(t-h(t))]^T,$$

$$e_i = \left[0_{n\times(i-1)n} \quad I \quad 0_{n\times(9-i)n}\right],$$

$$\Gamma_1 = \left[e_1 \quad he_5 \quad \frac{h^2}{2}e_6\right]^T, \Gamma_2 = [e_2 \quad e_1 - e_4 \quad h(e_1 - e_5)]^T,$$

$$G_0 = \begin{bmatrix} I & 0 & 0 & -I & 0 & 0 & 0 & 0 \\ I & 0 & 0 & I & -2I & 0 & 0 & 0 \\ I & 0 & 0 & -I & -6I & 0 & 0 & 0 \end{bmatrix}.$$

Theorem 1. *For given scalars $\bar{h}$, μ, ε_1, power system (24) is asymptotically stable with an H_∞ performance index $\gamma > 0$ if there exist real symmetric matrix $Z > 0$, $P > 0$, $Q_1 > 0$, $Q_2 > 0$, $Q_3 > 0$, $Q_4 > 0$, $R > 0$ and appropriate dimension matrix M, U such that as follows*

$$\Gamma = \begin{bmatrix} \Sigma_1 & \Sigma_2 & e_0^T C^T & \Theta D \\ 0 & -\frac{\varepsilon_1}{1+\mu} I_1 & 0 & 0 \\ 0 & 0 & -I_2 & 0 \\ 0 & 0 & 0 & 0 \\ 0 & 0 & 0 & -\gamma^2 I_3 \end{bmatrix} < 0, \tag{25}$$

$$N^T S^{-T} P = UC, \tag{26}$$

where

$$\Sigma_1 = \Lambda_1 - \Lambda_2 + \Lambda_3 + \Lambda_5 + \Lambda_6 + \Lambda_7 + \Lambda_8,$$

$$\Lambda_1 = 2\Gamma_1^T Z\Gamma_2 + e_1^T(Q_1+Q_2)e_1 - e_3^T Q_1 e_3 - e_4^T Q_2 e_4 + h^2 e_2^T R e_2,$$

$$\Lambda_2 = G_0^T \tilde{R} G_0, \tilde{R} = \mathrm{diag}\{R, 3R, 5R\},$$

$$\Lambda_3 = 2\Theta[(A+BKC)e_1 + A_d e_3 - e_2],$$

$$\Lambda_5 = \varepsilon_1 e_1^T M_1^T HH^T M_1 e_1 + \varepsilon_1 \mu e_2^T M_1^T HH^T M_1 e_2,$$

$$\Lambda_6 = 2e_7^T P\bar{S}^{-1}[A_h + 0.5NG_2 Ce_1] + e_7^T(Q_3+Q_4)e_7 - e_8^T Q_3 e_8 - e_9^T Q_4 e_9,$$

$$\Lambda_7 = 2\Theta BUe_7, \Lambda_8 = \frac{1+\mu}{\varepsilon_1} e_7 C^T K^T U^T E^T EUKCe_7,$$

$$\Sigma_2 = e_1^T C^T K^T E^T,$$

$$\Theta = e_1^T M_1^T + e_2^T \mu M_1^T,$$

$$A_h = (\bar{A} - \bar{L}_P\bar{C})e_7 + (\bar{A} - \bar{L}_H\bar{C})e_8.$$

Proof. The Lyapunov-functional is considered as

$$V(t) = V_x(t) + V_e(t), \tag{27}$$

where

$$V_x(t) = \eta^T(t)Z\eta(t) + \int_{t-h(t)}^{t} x(s)^T Q_1 x(s)ds + \int_{t-\bar{h}}^{t} x(s)^T Q_2 x(s)ds + \bar{h}\int_{t-\bar{h}}^{t}\int_{s}^{t} \dot{x}(s)^T R\dot{x}(s)dsdt$$

$$V_e(t) = 2e^T(t)P\dot{e}(t) + e^T(t)(Q_1 + Q_2)e(t) - e^T(t-h(t))Q_1 e(t-h(t)) - e^T(t-\bar{h})Q_2 e(t-\bar{h}).$$

Taking the derivation of $V(t)$, we have

$$\begin{aligned}\dot{V}_x(t) &= \varsigma^T(t)\Lambda_1\varsigma(t) - h^2\int_{t-\bar{h}}^{t} x^T(s)Rx(s)ds\\ \dot{V}_e(t) &= \varsigma^T(t)\Lambda_6\varsigma(t) + 2e_7^T P\bar{S}^{-1}[L_s u_s(t) - NG_1 f(t) - NG_2\varphi(t)].\end{aligned} \tag{28}$$

By Lemma 1, the integral term in (28) can be processed as

$$-h\int_{t-\bar{h}}^{t} x^T(s)Rx(s)ds \le -\varsigma^T(t)\Lambda_2\varsigma(t). \tag{29}$$

By applying free-weighting matrix technique [33], we have the following equality

$$2\left[x^T(t)M_1^T + \dot{x}^T(t)\mu M_1^T\right]\times[(A + (B + \Delta B(t))KC)x(t) + A_d x(t-h(t)) + (B+\Delta B(t))KCU\bar{e}(t) + Dw(t) - \dot{x}^T(t)] = 0. \tag{30}$$

Therefore, the Equation (30) can be expressed as

$$\varsigma^T(t)(\Lambda_3 + \Lambda_4 + \Lambda_7)\varsigma(t) + 2\varsigma^T(t)\Theta Dw(t) = 0. \tag{31}$$

By applying Lemma 2, we can obtain that

$$\begin{aligned}\Lambda_4 &= 2[e_1^T M_1^T + e_2^T\mu M_1^T]\times[\Delta B(t)KCe_1 + \Delta B(t)Ne_7]\\ &\le 2\varepsilon_1 e_1^T M_1^T Hg(t)g(t)H^T M_1 e_1 + \frac{1}{\varepsilon_1}(KCe_1 + KCUe_7)^T E^T E(KCe_1 + KCUe_7)\\ &\quad + 2\varepsilon_1\mu e_2^T M_1^T Hg(t)g(t)H^T M_1 e_2 + \frac{\mu}{\varepsilon_1}(KCe_1 + KCUe_7)^T E^T E(KCe_1 + KCUe_7)\\ &= \Lambda_5 + \Lambda_8 + \frac{1+\mu}{\varepsilon_1}e_1^T C^T K^T E^T EKCe_1.\end{aligned} \tag{32}$$

We define $L_s = \bar{S}P^{-1}C^T U^T$, $N^T S^{-T} P = UC$ and (29) can be processed as

$$\begin{aligned}2e_7^T P\bar{S}^{-1}[\bar{L}_s u_s(t) - NG_1\bar{f}(t) - NG_2\varphi(t)] &= 2e_7^T C^T U^T u_s(t) - 2e_7^T P\bar{S}^{-1}NG_1\bar{f}(t)\\ &\quad - 2e_7^T P\bar{S}^{-1}NG_2\varphi(t)\\ &\le -2\lambda \parallel s_e(t) \parallel .\end{aligned} \tag{33}$$

Combining (27) to (33), we can get

$$\dot{V} \le \varsigma(t)\Gamma\varsigma^T(t) - y^T(t)y(t) + \gamma^2 w^T(t)w(t). \tag{34}$$

If the matrix inequality (25) holds, the (34) can be processed as

$$\dot{V}(t) \le -y^T(t)y(t) + \gamma^2 w^T(t)w(t). \tag{35}$$

The integration of both sides of (35), we can get

$$V(+\infty) - V(0) \le \int_0^{\infty}\gamma^2 w^T(t)w(t)dt - \int_0^{\infty} y^T(t)y(t)dt. \tag{36}$$

Under initial condition $V(0) = 0$, the following inequality can be obtained

$$\int_0^{+\infty} y^T(t)y(t)dt \le \int_0^{\infty}\gamma^2 w^T(t)w(t)dt. \tag{37}$$

Hence, we have $\|y(t)\|_2 \le \gamma\|w(t)\|_2$ for $w(t) \ne 0$. Based on Definition 1, there exists a scalar $\epsilon > 0$ such that $\dot{V}(x(t)) \le -\epsilon\|\bar{x}(t)\|^2$. Therefore, the proposed active fault-tolerant LFC can guarantee the multi-area power system asymptotically stable. This completes the proof. □

Theorem 2. *For given scalars $\bar{h}$, μ, ε_1, if there exist real symmetric matrix $\bar{Z} > 0$, $P > 0$, $\bar{Q}_1 > 0$, $\bar{Q}_2 > 0$, $Q_3 > 0$, $Q_4 > 0$, $R > 0$ and matrix X, W, V, U, Y, Y_H such that as follows*

$$\bar{\Gamma}=\begin{bmatrix} \bar{\Sigma}_1 & \bar{\Sigma}_2 & e_1^T X^T C^T & \Theta D \\ 0 & -\frac{\varepsilon_1}{1+\mu} I_1 & 0 & 0 \\ 0 & 0 & -I_2 & 0 \\ 0 & 0 & 0 & 0 \\ 0 & 0 & 0 & -\gamma^2 I_3 \end{bmatrix} < 0, \tag{38}$$

$$\begin{bmatrix} -\sigma_1 I & (N^T S^{-T} P - UC)^T \\ 0 & -I \end{bmatrix} < 0, \tag{39}$$

$$\begin{bmatrix} -\sigma_2 I & (VC - CX)^T \\ 0 & -I \end{bmatrix} < 0, \tag{40}$$

where

$$\begin{aligned}
\bar{\Sigma}_1 &= \bar{\Lambda}_1 - \bar{\Lambda}_2 + \bar{\Lambda}_3 + \bar{\Lambda}_5 + \bar{\Lambda}_6 + \bar{\Lambda}_7 + \bar{\Lambda}_8,\\
\bar{\Lambda}_1 &= 2\Gamma_1^T \bar{Z}\Gamma_2 + e_1^T(\bar{Q}_1 + \bar{Q}_2)e_1 - e_2^T \bar{Q}_1 e_2\\
&\quad - e_3^T \bar{Q}_2 e_3 + h^2 e_2^T \bar{R} e_2,\\
\bar{\Lambda}_2 &= G_0^T \hat{R} G_0, \hat{R} = \mathrm{diag}\{\bar{R}, 3\bar{R}, 5\bar{R}\},\\
\bar{\Lambda}_3 &= 2\bar{\Theta}[(\bar{A} + \bar{B}\bar{K}\bar{C})e_1 + \bar{A}_d \bar{X} e_3 - \bar{X} e_2],\\
\bar{\Lambda}_5 &= \varepsilon_1 e_1^T \bar{H}\bar{H}^T e_1 + \varepsilon_1 \mu e_2^T \bar{H}\bar{H}^T e_2,\\
\Lambda_6 &= 2e_7^T \bar{P}\bar{S}^{-1}[\bar{A}_b + 0.5\bar{N}G_2 C e_1] + e_7^T(Q_3 + Q_4)e_7\\
&\quad - e_8^T Q_3 e_8 - e_9^T Q_4 e_9,\\
\bar{\Lambda}_7 &= 2\bar{\Theta}\bar{B}\bar{U}e_7, \Lambda_8 = \frac{1+\mu}{\varepsilon_1} e_7 U^T E^T E U e_7,\\
\Sigma_2 &= e_1^T X^T C^T K^T E^T,\\
\bar{\Theta} &= e_1^T + e_2^T \mu,\\
\bar{A}_b &= (\bar{A} - \bar{L}_P \bar{C})e_7 + (\bar{A} - \bar{L}_H \bar{C})e_8.
\end{aligned}$$

Then the power system (24) is asymptotically stable with an H_∞ performance index $\gamma > 0$, the controller gain $K = WV^{-1}$ and the observer gain $\bar{L}_P = \bar{S}P^{-1}Y$, $\bar{L}_H = \bar{S}P^{-1}Y_H$, $\bar{L}_S = \bar{S}P^{-1}C^T U^T$.

Proof. By defining $X = M^{-1}$, $\bar{Z} = XZX$, $\bar{Q}_1 = XQ_1X$, $\bar{Q}_2 = XQ_2X$, $\bar{R} = XRX$, and pre- and post-multiplying both side of (25) with $\mathrm{diag}\{X, X, \cdots, I, I, I, I\}$, we can obtain (38). What is more, for $\bar{B}\bar{K}\bar{C}$, $\bar{E}\bar{K}\bar{C}$, it is difficult to find observer gain K because the matrix C is not invertible. Following the method in [20], above problem can be transformed a minimization issue. By defining $WC = KCX$, $VC = CX$, we can get

$$(VC - CX)^T (VC - CX) = 0$$

It can be further converted into (40) by using the Lemma 1 and the same can be found in (39). Hence the controller gain matrix K can be described as $K = WV^{-1}$. This completes the proof. □

Remark 3. This paper mainly proposes LMI-based LFC. Compared with the pole assignment method, we don't require a set of expected poles to calculate the controller gain. The controller gain $K = WV^{-1}$, observer gain $\bar{L}_P = \bar{S}P^{-1}Y$, $\bar{L}_H = \bar{S}P^{-1}Y_H$, and $\bar{L}_S = \bar{S}P^{-1}C^T U^T$ are obtained by solving the LMI matrices in Theorem 2, which can be found in [23, 25].

3.4 | Reachability of the sliding mode surface

In this subsection, in order to ensure the accessibility of the sliding surface in the error estimation space, the following theorem is proposed.

Theorem 3. *If there exist parameter matrix U and matrices P with appropriate dimension such that the constraints (38), (39) and (40) hold, the sliding mode input $u_s(t)$ guarantees the sliding motion to be driven to the sliding mode surfaces $s_e = 0$ in a finite time.*

Proof. Defining $F = NS^{-T}$, the Lyapunov-functional can be considered as

$$V(t) = 0.5 s_e^T \left(FPF^T\right)^{-1} s_e. \tag{41}$$

Taking the derivation of the constructed Lyapunov function, we can get

$$\begin{aligned}
\dot{V}(t) =& s_e^T (FPF)^{-1} FPS^{-1} \times [(\bar{A} - \bar{L}_P \bar{C})\bar{e}(t)\\
&+ (\bar{A} - \bar{L}_H \bar{C})\bar{e}(t - \tau(t)) - NG_1 \bar{f}(t)\\
&+ aNG_2 Cx(t) - NG_2 \varphi(t) + \bar{L}_s u_s(t)].
\end{aligned} \tag{42}$$

Using $L_s = \bar{S}P^{-1}C^T U^T$ and $N^T S^{-T} P = UC$, we can get

$$\begin{aligned}
&s_e^T (FPF)^{-1} FPS^{-1}\\
&\times \left[\bar{L}_s u_s(t) - NG_1 \bar{f}(t) - NG_2 \varphi(t)\right]\\
&\le s_e^T \left[u_s(t) - G_1 \bar{f}(t) - G_2 \varphi(t)\right]\\
&\le -\lambda \parallel s_e \parallel .
\end{aligned} \tag{43}$$

Combining (42) and (43), we can get

$$\begin{aligned}
\dot{V}(t) \le& -\|s_e(t)\|\{\lambda - \|(FPF)^{-1} FP\bar{S}^{-1}(\bar{A} - \bar{L}_p \bar{C})\|\\
&\times \|\bar{e}(t)\| - \|(FPF)^{-1} FP\bar{S}^{-1} aNG_2\|y(t))\|\\
&- \|(FPF)^{-1} FP\bar{S}^{-1}(\bar{A} - \bar{L}_b \bar{C})\|\|\bar{e}(t - h(t))\|\}.
\end{aligned} \tag{44}$$

Using Theorem 1, we can get $\|y(t)\| \le \gamma \|w(t)\|$, then we define

$$\varphi = \|(FPF)^{-1} FP\bar{S}^{-1}(\bar{A} - \bar{L}_p \bar{C}), \tag{45}$$

$$\psi = \|(FPF)^{-1}FP\bar{S}^{-1}(\bar{A} - \bar{L}_{\beta}\bar{C})\|, \tag{46}$$

$$\xi = \|(FPF)^{-1}FP\bar{S}^{-1}aNG_2\|. \tag{47}$$

From (45) to (47), we can obtained

$$\dot{V}_s(t) \leq -\|s_e(t)\|\{\lambda - \xi\gamma\|w(t)\| - \varphi\|\bar{e}(t)\| - \psi\|\bar{e}(t - h(t))\|\}. \tag{48}$$

Then, we define the following domain as

$$\Omega \triangleq \bigcap_{i=1}^{s} \Omega(\xi, \varphi, \psi), \tag{49}$$

$$\Omega(\xi, \varphi, \psi) \triangleq \{\lambda - \xi\gamma\|w(t)\| - \varphi\|\bar{e}(t)\| - \psi\|\bar{e}(t - h(t))\| > 0\}. \tag{50}$$

From (49) and (50), it is noticed that $\dot{V}(t) < 0$ is in the domain Ω. Furthermore, we have proved the stabilization of (25) in Theorem 1. This implies that the trajectories of $\bar{e}(t)$ will enter Ω in finite time and remains thereafter. Until now, we complete the proof. □

4 | NUMERICAL EXAMPLES

In this section, four cases are provided to verify the effectiveness of the proposed active fault-tolerant LFC in the multi-area power system with sensors faults and deception attacks. A three-area power system model with EVs is established on the Matlab/Simiulink environment.

The first one illustrates that the proposed active fault-tolerant LFC can guarantee the stability of the power system under deception attacks and sensor faults. The second one studies the sensitivity analysis of the proposed active fault-tolerant LFC with respect to the parameters. The third one studies that the proposed active fault-tolerant LFC strategy has been compared with the other LFC methods subject to the same condition. We test the proposed active fault-tolerant LFC on IEEE 39-bus system in the fourth one.

The parameters of the three-area power system are shown in Table 2, which are similar to [25, 35]. What is more, defined the $T_{12} = 0.03$, $T_{23} = 0.02$, $T_{13} = 0.035$, the upper bound of time-varying delay $\bar{h} = 0.01$ s.

The number of EVs $N(t)$ participating in LFC is shown in Figure 3. It can be seen that N change with time. The SOC parameters of EVs are $SOC_{min,i} = 10\%$, $SOC_{high,i} = 85\%$. Therefore, combine (7), the aggregated EVs gain is shown in Figure 3.

Example 1. We design the active fault-tolerant LFC to ensure the stability of the closed loop system (24) under deception attack and sensor fault.

TABLE 2 Parameters of each area.

Parameter	Area1	Area2	Area3
M_i	0.12	0.1	0.08
D_i	2	1.5	2
R_i	2	1	1.8
T_{mi}	0.5	0.5	0.55
T_{gi}	0.15	0.25	0.2
T_{ei}	1	1	1
K_{mi}	1	1	1
ε_i	0.1	0.11	0.1

The deception attack is defined as $\varphi(t) = 0.01\sin(1.8t)$ and $\nu = 0.01$, therefore

$$f_{ag}(t) = \begin{cases} -0.5Cx(t) + 0.01\sin(1.8t) & |\Delta f_i| < 0.01 \\ 0 & otherwise \end{cases}. \tag{51}$$

Assuming that the fault time is from $t = 5s$ to $t = 12s$ and the sensor fault is shown in Figure 4. We choose $\alpha_1 = \alpha_2 = \alpha_3 = 0.6, \sigma_1 = \sigma_2 = \sigma_3 = 0.02$, the adjustable parameters $\lambda_1 = \lambda_2 = \lambda_3 = 1$. The sliding mode input $u_s(t)$ is designed as

$$u_{s1}(t) = u_{s2}(t) = u_{s3}(t) = (-0.5 + G_1 0.6 + G_2 0.02)sgn(s_e(t))$$

The observer gain L_D is designed as

$$L_{D1} = L_{D2} = L_{D3} = \begin{bmatrix} 0 & 0 & 0 & 0 & 0 & 0 & 1 & 0 & 1 \\ 0 & 0 & 0 & 0 & 0 & 0 & 0 & 1 & 1 \end{bmatrix}.$$

Based on the Theorem 2, the observer gain L_P, L_H and controller gain K can be obtained by the MATLAB toolbox.

$$L_{P1} = \begin{bmatrix} -3.23 & 4.06 & -12.81 & 0.32 & -0.11 & -0.72 \\ 4.34 & 32.40 & 62.90 & 1.04 & 1.81 & 21.41 \\ -278.43 & -25.89 & -2.47 \\ 517.20 & 44.62 & 23.14 \end{bmatrix},$$

$$L_{P2} = \begin{bmatrix} -3.27 & 5.66 & -12.16 & 0.29 & -0.12 & -0.67 \\ 4.01 & 31.80 & 59.39 & 1.09 & 1.79 & 20.69 \\ -280.65 & -25.58 & -2.13 \\ 496.50 & 41.70 & 21.45 \end{bmatrix},$$

$$L_{P3} = \begin{bmatrix} -2.95 & 9.67 & -12.22 & 0.24 & -0.16 & -1.40 \\ 3.87 & 40.67 & 65.41 & 1.48 & 2.10 & 25.19 \\ -304.16 & -27.04 & -2.54 \\ 569.37 & 45.82 & 25.00 \end{bmatrix},$$

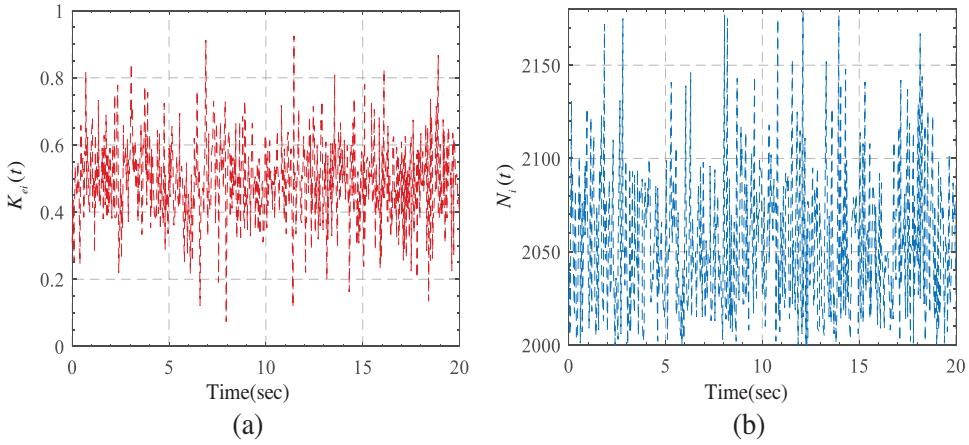

FIGURE 3 (a) Aggregated EVs gain $K_{ei}(t)$; (b) number of EVs $N(t)$.

FIGURE 4 The sensor fault of power system.

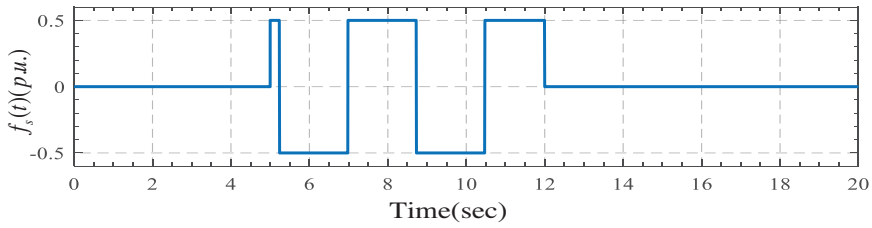

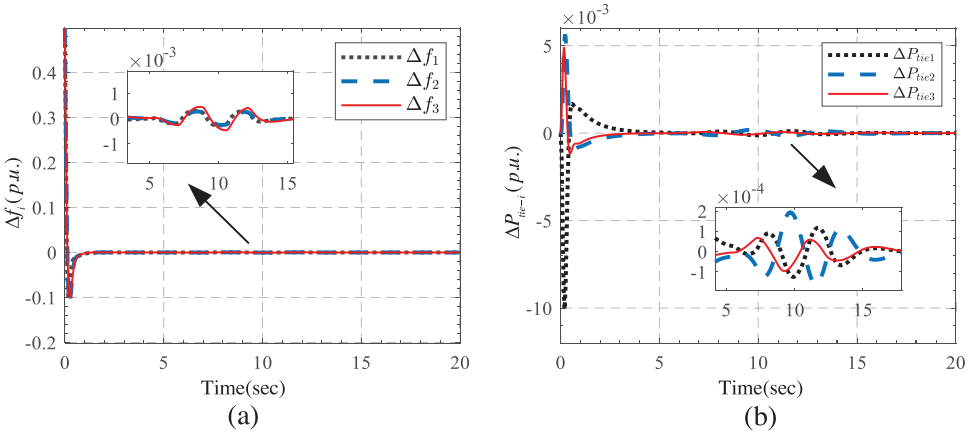

FIGURE 5 (a) The frequency deviation Δf_i; (b) the tie-line power ΔP_{tie-i}.

$$L_{H1}=\begin{bmatrix} 0_{2\times1} & 0_{2\times1} \\ 0 & -1.43 \\ 0_{6\times1} & 0_{6\times1} \end{bmatrix}^T, L_{H2}=\begin{bmatrix} 0_{2\times1} & 0_{2\times1} \\ 0 & -1.42 \\ 0_{6\times1} & 0_{6\times1} \end{bmatrix}^T,$$

$$L_{H3}=\begin{bmatrix} 0_{2\times1} & 0_{2\times1} \\ 0 & -1.47 \\ 0_{6\times1} & 0_{6\times1} \end{bmatrix}^T.$$

The system estimates obtained by the observer were used for controller design, and the system controller gain as

$$K_1=\begin{bmatrix} -1.02 \\ -9.23 \end{bmatrix}^T, K_2=\begin{bmatrix} -1.08 \\ -9.34 \end{bmatrix}^T, K_3=\begin{bmatrix} -1.15 \\ -8.91 \end{bmatrix}^T.$$

We take the frequency deviation and the deviation of the tie-line power as examples. The simulative results of the three-area power system are shown in Figure 5. Therefore, it can be seen that the proposed active fault-tolerant LFC can effectively

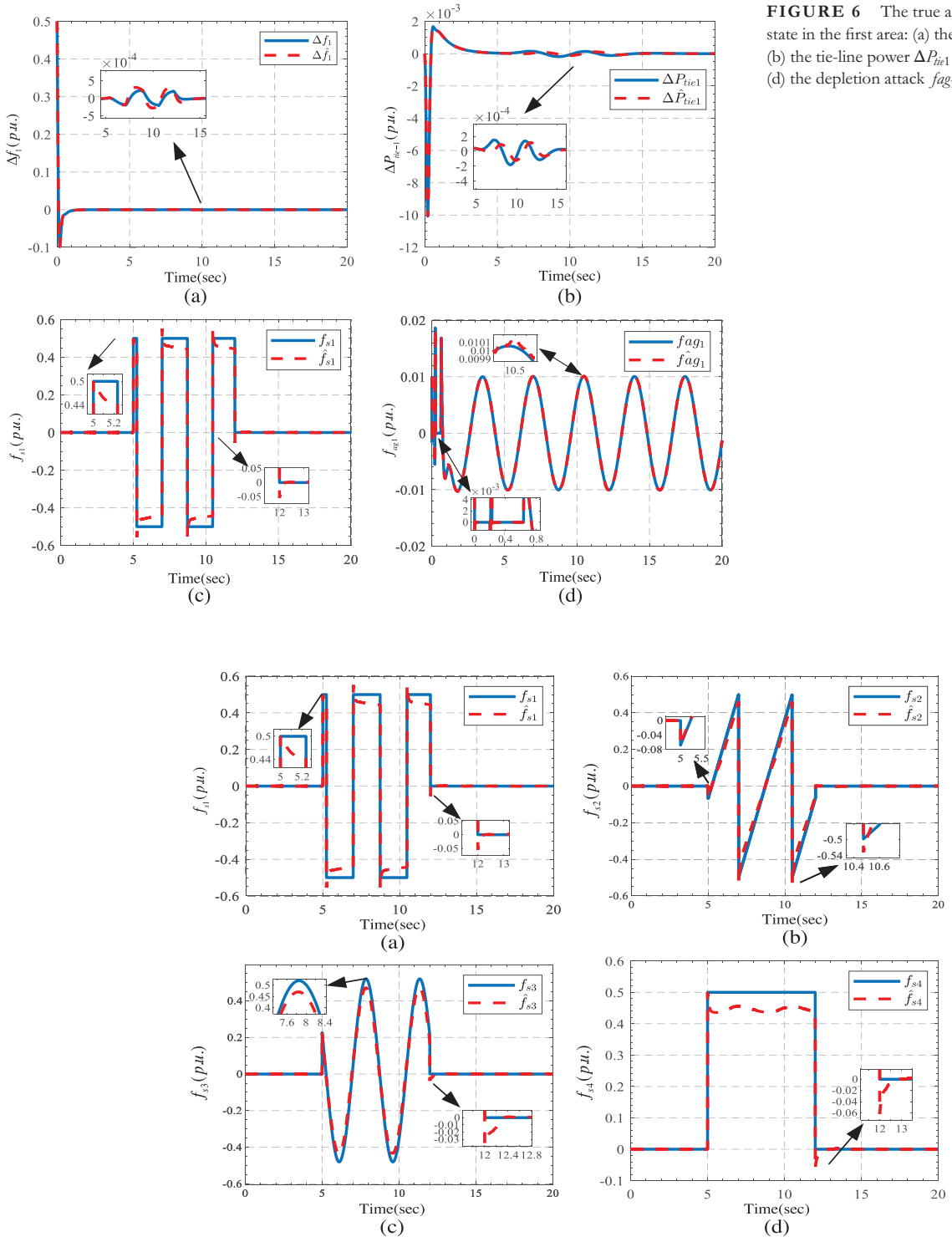

FIGURE 6 The true and the estimated system state in the first area: (a) the frequency deviation Δf_1; (b) the tie-line power ΔP_{tie1}; (c) the sensor fault f_{s1}; (d) the depletion attack fag_1.

FIGURE 7 The true and the estimated sensor faults in the first area: (a) a square wave fault signal; (b) a triangular wave fault signal; (c) a sinusoidal fault signal; (d) a rectangular wave fault signal.

ensure the stability of the system. We take the first area as an example. Figure 6 shows the true and the estimated system state. In Figure 6, the proposed observer can quickly and accurately estimates the system state.

To further illustrate the effectiveness of the proposed PD sliding mode observer, we consider four different fault signals occurring in the system. We take the first area as an example. The true and the estimated sensor faults are shown in Figure 7.

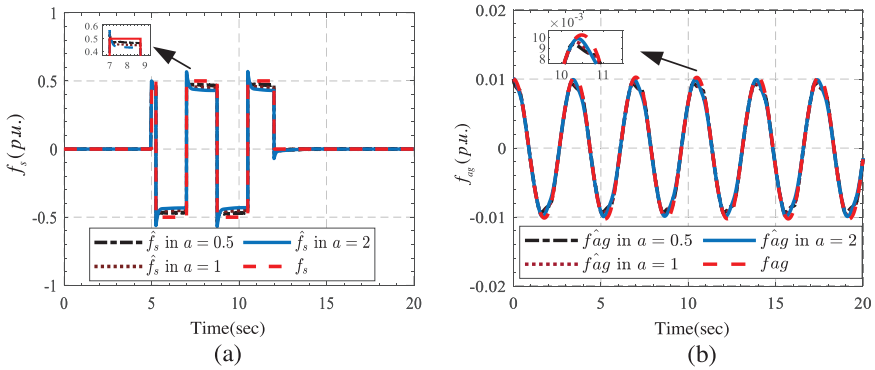

FIGURE 8 The comparisons of observer performance under different parameters.

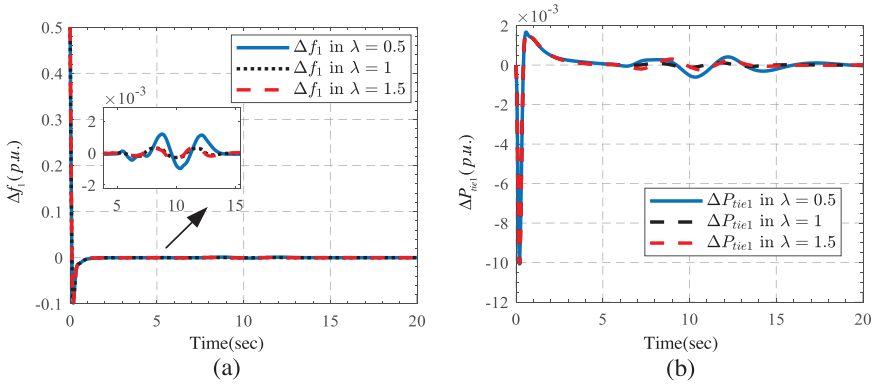

FIGURE 9 The comparisons of system state under different parameters: (a) the frequency deviation Δf_i; (b) the tie-line power ΔP_{tie-i}.

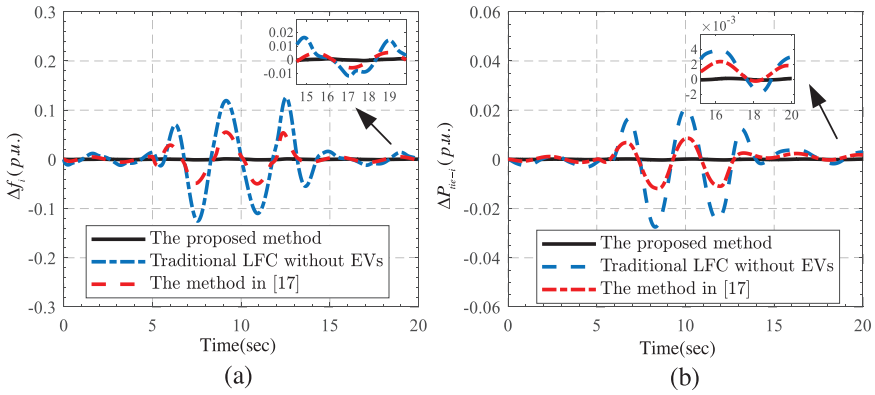

FIGURE 10 (a) The frequency deviation Δf_i; (b) the tie-line power ΔP_{tie-i}.

It is obvious that the proposed observer can effectively deal with different types of fault signals.

Example 2. We study the sensitivity analysis of the proposed active fault-tolerant LFC with respect to the some parameters.

The parameters of the system are identical to Example 1. Firstly, the observer gain $\bar{L}_D$ can be expressed as:

$$\bar{L}_D = \begin{bmatrix} 0 & 0 & 0 & 0 & 0 & 0 & a & 0 & a \\ 0 & 0 & 0 & 0 & 0 & 0 & 0 & a & a \end{bmatrix}.$$

The comparison of observer performance with different parameters are shown in Figure 8.

Then we study effect of different parameter λ_i on the power system. The comparison of Δf_i and ΔP_{tie-i} with different parameters λ_i are shown in Figure 9.

Example 3. The proposed active fault-tolerant LFC scheme is compared with the LFC used in [17] and the traditional LFC without EVs.

The parameters of the system are identical to Example 1. The simulated results are shown in Figure 10. It can be seen that the method in [17] is difficult to avoid the interference of sensor fault and deception attack. Therefore, it makes the frequency deviation and the deviation of the tie-line power have a large deviation. However, the proposed active fault-tolerant LFC scheme can guarantee the stability of the power system. In

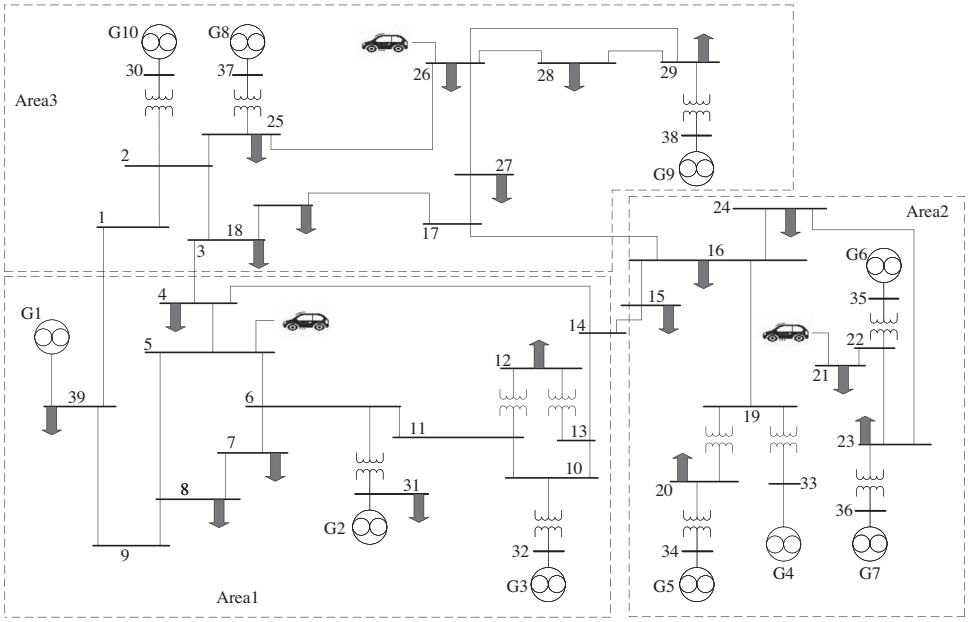

FIGURE 11 Single-line diagram of IEEE 39-bus system.

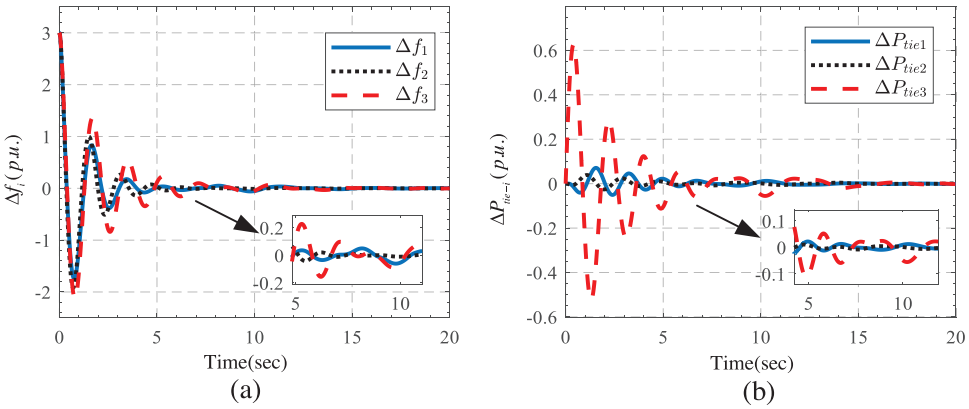

FIGURE 12 (a) The frequency deviation Δf_i; (b) the tie-line power ΔP_{tie-i}.

addition, the existence of EVs can effectively reduce the power oscillations.

Example 4. We test the proposed scheme on IEEE 39-bus system. The IEEE 39-bus test system is shown in Figure 11. The system consists of 10 generators, 19 loads, 34 transmission lines, and 12 transformers [36]. The power system is divided into three areas. Furthermore, three EVAs are introduced in buses 5, 21 and 26, respectively.

Here, the parameters including the participation factor of every governor are given in Table 3, which can be found in [37]. The values of deception attacks and sensor faults are identical to Example 1.We take frequency deviation and the deviation of the tie-line power as examples. The simulated results of the IEEE 39-bus system are shown in Figure 12. It can be seen that

TABLE 3 Parameters of each area.

Parameter	Area1	Area2	Area3
M_i	10	10	11
D_i	4	3.5	4
R_i	3	3.5	4
T_{mi}	0.05	0.04	0.03
T_{gi}	0.03	0.03	0.03
T_{ei}	1	1	1
K_{mi}	1	1	1
ε_i	0.1	0.11	0.1
Area1	$\alpha_{11_g} = 0.3, \alpha_{12_g} = \alpha_{13_g} = 0.2, \alpha_{11_e} = 0.3$		
Area2	$\alpha_{21_g} = 0.3, \alpha_{22_g} = \alpha_{23_g} = 0.2, \alpha_{21_e} = 0.3$		
Area2	$\alpha_{31_g} = \alpha_{32_g} = \alpha_{33_g} = \alpha_{34_g} 0.2, \alpha_{31_e} = 0.2$		

the proposed active fault-tolerant LFC scheme can effectively guarantee the stability of the IEEE 39-bus system.

5 | CONCLUSION

This paper studied the stability of multi-area power systems with EVs under sensor faults and deception attacks. A multi-area power system model has been proposed under sensor faults and deception attacks with the uncertainty of electric vehicle battery status. An active fault-tolerant LFC scheme has been presented to ensure the stability of the multi-area power systems. The simulation with respect to a three-area power system has verified the effectiveness of the proposed active fault tolerant load frequency control in this paper.

AUTHOR CONTRIBUTIONS

Xinghua Liu: Conceptualization, methodology, supervision, writing - original draft, writing - review and editing. Yuru Liang: Formal analysis, investigation, writing - original draft. Siwei Qiao: Software, validation, writing - review and editing. Guoqing Yang: Conceptualization, investigation, supervision, writing - review and editing. Peng Wang: Conceptualization, supervision, writing - review and editing.

ACKNOWLEDGEMENTS

This work was supported in part by the National Natural Science Foundation of China (Grant No. U2003110), and in part by the High Level Talents Plan of Shaanxi Province for Young Professionals.

CONFLICT OF INTEREST STATEMENT

The authors declare no conflict of interests.

DATA AVAILABILITY STATEMENT

The data that support the findings of this study are available on request from the corresponding author. The data are not publicly available due to privacy or ethical restrictions.

ORCID

Xinghua Liu https://orcid.org/0000-0001-5665-3535

REFERENCES

1. Prakash, M., Hoon, J.Y.: Fuzzy logic-based integral sliding mode control of multi-area power systems integrated with wind farms. Inf. Sci. 545, 153–169 (2021)
2. Sofia, A.B., Gerardo, E.P., Danilo, M.O., Alejandro, G.: Passivity-based control of islanded microgrids with unknown power loads. IMA J. Math. Control Inf. 37(4), 1548–1573 (2020)
3. Chen, P., Zhang, D., Li, Y., Yan, H.: Dynamic event-triggered output feedback control for load frequency control in power systems with multiple cyber attacks. IEEE Trans. Syst. Man Cybern.: Syst. 52(10), 6246–6258. https://doi.org/10.1109/TSMC.2022.3143903.
4. Hossain, M.M., Peng, C., Wang, Y.L., Du, X.: Handshake Logic-Based Event-Triggered Load Frequency Control for Smart Grids Under DoS Attacks. IEEE Trans. Ind. Inf. 18(6), 3863–3872 (2022)
5. Lv, X., Zhai, S., Sun, Y., Hou, D., Wang, S.: Load frequency control for multi-area power system based on Markov model. J. Franklin Inst. 358, 8377–8395 (2021)
6. Mahendran, M.V., Vijayan, V.: Model-predictive control-based hybrid optimized load frequency control of multi-area power systems. IET Gener. Transm. Distrib. 15, 1521–1537 (2021)
7. Khan, M., Sun, H., Xiang, Y., Shi, D.: Electric vehicles participation in load frequency control based on mixed H_2/H_∞. Int. J. Electr. Power Energy Syst. 125, 106420–106430 (2021)
8. Sitthidet, V., Issarachai, N.: Robust LFC in a smart grid with wind power penetration by coordinated V2G control and frequency controller. IEEE Trans. Smart Grid 5, 371–380 (2014)
9. Chao, L., Bi, T., Marija, I., Kevin, T., Wang, X.: Guest editorial: new trends in wide-area monitoring and control of power systems with large scale renewables. IET Gener. Transm. Distrib. 11, 4403–4405 (2017)
10. Seok, K.K., Keun, S.D.: The effect of EV aggregators with time-varying delays on the stability of a load frequency control system. IEEE Trans. Syst. Man Cybern.: Syst. 33(1), 669–680 (2017)
11. Evangelos, L.K., Kostas, A.P., Nikos, D.H.: Distributed coordination of electric vehicles providing V2G regulation services. IEEE Trans. Syst. Man Cybern.: Syst. 31(4), 2834–2846 (2016)
12. Zeng, H., Zhou, S., Zhang, X., Wang, W.: Delay-dependent stability analysis of load frequency control systems with electric vehicles. IEEE Trans. Cybern. 52(12), 13645–13653. https://doi.org/10.1109/TCYB.2022.3140463
13. Ngoc, P.T., Than, O.A.M., Hieu, T.: Event-triggered mechanism for multiple frequency services of electric vehicles in smart grids. IEEE Trans. Syst. Man Cybern.: Syst. 37(2), 967–981 (2021)
14. Aravindh, D., Sakthivel, R., Kaviarasan, B., Marshal, S.A., Faris, A.: Design of observer-based non-fragile load frequency control for power systems with electric vehicles. ISA Trans. 91, 21–31 (2019)
15. Wang, Z., Liu, Y., Yang, Z., Yang, W.: Load frequency control of multi-region interconnected power systems with wind power and electric vehicles based on sliding mode control. Energies 14(8), 2288–2298 (2021)
16. Santosh, T., Vijay, S., Nand, K., Pandey, A.: Load frequency control of power system considering electric vehicles' aggregator with communication delay. Int. J. Electr. Power Energy Syst. 145, 108697–108706 (2023)
17. Ngoc, P.T., Saeid, N., Hieu, T., Po, W.K.: Static output feedback frequency stabilization of time-delay power systems with coordinated electric vehicles state of charge control. Int. J. Electr. Power Energy Syst. 32(5), 3862–3874 (2016)
18. Arunagirinathan, S., Muthukumar, P., Joo, Y.H.: Robust reliable H_∞ control design for networked control systems with nonlinear actuator faults and randomly missing measurements. Int. J. Robust Nonlinear Control 29(12), 4168–4190 (2019)
19. Ali, S.M., Babak, M., Soodabeh, S., Mahdian, D.N., Mohammadnezhad, S.H., Josep, G.M.: Distributed consensus-based fault tolerant control of islanded microgrids. IEEE Trans. Smart Grid 11(1), 37–47 (2019)
20. Liang, X., Wang, Q., Hu, C., Dong, C.: Observer-based H_∞ fault-tolerant attitude control for satellite with actuator and sensor faults. Aerosp. Sci. Technol. 95, 105424–105433 (2019)
21. Sharmila, V., Rakkiyappan, R., Hoon, J.Y.: Fuzzy sampled-data control for DFIG-based wind turbine with stochastic actuator failures. IEEE Trans. Syst. Man Cybern.: Syst. 51(4), 2199–2211 (2019)
22. Satadru, D., Sara, M., Pierluigi, P., Beshah, A.: Sensor fault detection, isolation, and estimation in lithium-ion batteries. IEEE Trans. Control Syst. Technol. 24(6), 2141–2149 (2016)
23. Subramanian, K., Hoon, J.Y., Sol, K.H.: Fault-tolerant load frequency control for DFIG-based interconnected wind power systems. Inf. Sci. 582, 73–88 (2022)
24. Kaviarasan, B., Sakthivel, R., Kwon, O.: Robust fault-tolerant control for power systems against mixed actuator failures. Nonlinear Anal. Hybrid Syst. 22, 249–261 (2016)
25. Su, X., Liu, X., Song, Y.: Fault-tolerant control of multiarea power systems via a sliding-mode observer technique. IEEE/ASME Trans. Mechatron. 23(1), 38–47 (2017)

26. Zhou, X., Dou, Z., Zhang, W., et al.: Distributed sliding mode fault-tolerant LFC for multiarea interconnected power systems under sensor fault. Complexity 2022, 6271232 (2022)
27. Athira, M., Nader, M., Hasan, M.: A comprehensive review of the cyber-attacks and cyber-security on load frequency control of power systems. Energies 13(15), 3860–3870 (2020)
28. Zhang, X., Yang, F., Sun, X.: Resilient adaptive event-triggered load frequency control of network-based power systems against deception attacks. Sensors 21(21), 7047–7057 (2021)
29. Tian, E., Peng, C.: Memory-based event-triggering H_∞ load frequency control for power systems under deception attacks. IEEE Trans. Cybern. 50(11), 4610–4618 (2020)
30. Liu, J., Gu, Y., Zha, L., Liu, Y., Cao, J.: Event-triggered H_∞ load frequency control for multiarea power systems under hybrid cyber attacks. IEEE Trans. Syst. Man Cybern.: Syst. 49, 1665–1678 (2019)
31. Wang, X., Ding, D., Dong, H., Yi, X.: PI-based security control against joint sensor and controller attacks and applications in load frequency control. IEEE Trans. Syst. Man Cybern.: Syst. 53(2), 970–980. doi:10.1109/TSMC.2022.3190005.
32. Alexandre, S., Frederic, G.: Wirtinger-based integral inequality: Application to time-delay systems. Automatica 49(9), 2860–2866 (2013)
33. Zhang, X., Li, M., Wu, M., She, J.: Further results on stability and stabilisation of linear systems with state and input delays. Int. J. Syst. Sci. 40(1), 1–10 (2009)
34. Yin, S., Yang, H., Kaynak, O.: Sliding mode observer-based FTC for Markovian jump systems with actuator and sensor faults. IEEE Trans. Autom. Control 62(7), 3551–3558 (2017)
35. Peng, C., Zhang, J., Yan, H.: Adaptive Event-Triggering H_∞ Load Frequency Control for Network-Based Power Systems. IEEE Trans. Ind. Electron. 65(2), 1685–1694 (2018)
36. Hiskens, I.: IEEE PES task force on benchmark systems for stability controls. Technical Report pp. 1–23. (2013)
37. Yan, C.H., Liu, B., Xiao, P., Zhang, C.: Stabilization of Load Frequency Control System via Event-Triggered Intermittent Control. IEEE Trans. Circuits Syst. II Exp. Briefs 69(12), 4934–4938 (2022)

How to cite this article: Liu, X., Liang, Y., Qiao, S., Yang, G., Wang, P.: Active fault-tolerant load frequency control for multi-area power systems with electric vehicles under deception attacks. IET Control Theory Appl. 18, 109–124 (2024). https://doi.org/10.1049/cth2.12544